Highlights

A Regional Hydrological Model for Arid and Semi-Arid River Basins with Consideration of Irrigation

Cong Jiang, Eric J. R. Parteli, Qian Xia, Xin Yin, Yaping Shao

- We introduce a new irrigation model for regional hydrological simulations.
- Our irrigation model considers off-stream water flux over long distances from the river to irrigation districts.
- We explicitly model the actual irrigation amount from soil moisture deficit, water availability and irrigation fraction.
- GRACE data are considered in the model verification and assessment.
- Our irrigation model provides a useful tool for hydrological modelling in arid and semi-arid basins.

A Regional Hydrological Model for Arid and Semi-Arid River Basins with Consideration of Irrigation

Cong Jiang[a,*], Eric J. R. Parteli[b], Qian Xia[c], Xin Yin[a] and Yaping Shao[a]

[a]*Institute for Geophysics and Meteorology, University of Cologne, Pohligstr. 3, Cologne, 50969, North Rhine-Westphalia, Germany*
[b]*Faculty of Physics, University of Duisburg-Essen, Duisburg, Lotharstr. 1, 47057, North Rhine-Westphalia, Germany*
[c]*School of Water Resources and Hydropower Engineering, Wuhan University, Bayi road. 299, 430072, Hubei Province, China*

ARTICLE INFO

Keywords:
Hydrological Modelling,
Yellow River Basin, Arid and Semi-arid Areas,
Irrigation Model,
Calibration,
Validation

ABSTRACT

We develop a regional hydrological model that applies to arid and semi-arid regions, by explicitly considering the effect of irrigation on the hydrological processes. A new irrigation module is here integrated into the recently introduced Atmospheric and Hydrological Modelling System (AHMS) for the quantitative assessment of basin-scale hydrological response to climate change and the impact of anthropogenic activities on water resources. The land surface, channel routing and groundwater modules of the AHMS are extended here to incorporate the new module. We then apply the model to simulating the hydrological processes in the Yellow River Basin, an arid and semi-arid region where irrigation constitutes the most important source of water use. The model is calibrated and validated using in-situ and remote sensing observations. This study demonstrates the capability of the AHMS for regional hydrological modelling in arid and semi-arid basins where irrigation profoundly influences the water balance.

1. Introduction

Atmospheric and hydrological models have been under intensive development in recent years, as they provide a powerful tool for the assessment and prediction of regional hydrological processes and the investigation of the dynamic feedbacks between the atmosphere and continental hydrosphere (Gochis et al., 2013; Maxwell et al., 2011; Shrestha et al., 2014; Wagner et al., 2016). Such models have found diverse applications in studies on basin-scale hydrological responses to climate change and anthropogenic activities (Maxwell et al., 2007; Wilby et al., 1994).

However, hydrological simulation in arid and semi-arid regions remains a formidable task, because the reliable representations of the often low and heterogeneous rainfall, intermittent river flow and impacts of human activities, are particularly challenging (Pilgrim et al., 1988; Rafiei-Sardooi et al., 2022). Thus, we focus here on the development of a hydrological model for arid and semi-arid regions. Specifically, the Yellow River Basin is selected as the research area owing to its unique hydrological characteristics and important position in China. The Yellow River is the second-longest river in China (5464 km) and the Yellow River Basin (795,000 km^2) is the largest basin in north China. The average water resources in the Yellow River Basin account for only 2 % of the total water resources in China, but the water from this basin feeds 12% of the Chinese population. However, water shortage constitutes a serious problem given the increasing water demand in the area, with continuing population growth and urban development. In 1997, the downstream 704 kilometers from the estuary dried up for more than 226 days (Cong et al., 2009). The large irrigation districts in the Yellow River Basin are mainly located in arid and semi-arid areas, and irrigation has accounted, for instance, for more than 80% (60%) of the gross human water use in the period from 1956 to 2010 (2001-2019) and rapidly increasing with time (Fig. 1). For instance, Hetao region takes about 5 billion m^3 water every year from the Yellow River.

Although industrial water use has been increasing since the early 2000s due to economic development, irrigation still constitutes the most important source of water use in this area (Jia et al., 2006). Most previous studies about hydrological processes in the Yellow River Basin neglected explicit consideration of river water use in large-scale irrigation districts (e.g. Cong et al., 2009,

*Corresponding author

c.jiang@uni-koeln.de (C. Jiang)
ORCID(s): 0000-0002-2405-6645 (C. Jiang)

Yuan et al., 2016). A water use module was introduced in the WEP-L distributed hydrological model by Jia et al. (2006), by taking the census irrigation data as input, assess the water resources in the Yellow River Basin. In the latter study, irrigation water requirements in the model were estimated using statistical methods and data, not physically based modelling.

Yin et al. (2021) extended the global land surface model ORCHIDEE (ORganizing Carbon and Hydrology in Dynamic EcosystEms) by including a model for irrigation, crop and offline dam operation. Their model assumes that streams supply water to the crops within the grid cells they flow across only, neglecting water transfer over long distances. Given the commonly used channels in the irrigation districts of arid and semi-arid regions, this neglect may lead to an underestimation of actual river irrigation volumes and affect the accuracy of hydrological simulations over large irrigated districts (Yin et al., 2021).

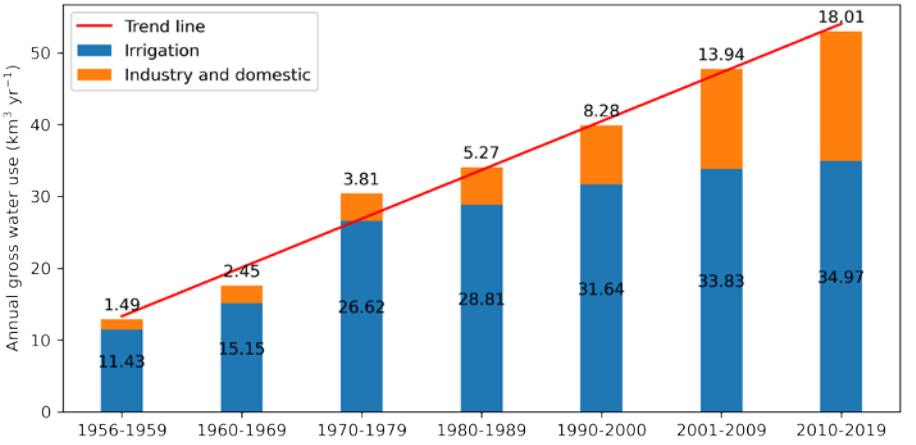

Figure 1: Annual gross water use in the Yellow River Basin from 1956 to 2019. For the period from 1956 to 2000, data were obtained from Jia et al. (2006), while for the period 2001-2019, data were collected from the Yellow River Bulletin of Water Resources, published by the Yellow River Conservancy Commission (YRCC) of the Ministry of Water Resources of China (http://www.yrcc.gov.cn/other/hhgb/).

The main purpose of this article is to develop a hydrological model for long-term, large-scale hydrological processes in arid and semi-arid basins, focusing on the Yellow River Basin. Our model development builds on the offline mode of the coupled Atmospheric and Hydrological Modelling System (AHMS), developed at the University of Cologne (Jiang et al., 2020; Xia, 2019). An example of the AHMS applications to wet hydrological basins can be found in Xia et al. (2022). The use of river water and groundwater for irrigation in the Yellow River Basin is expected to profoundly impact the regional hydrological processes. We thus extend the AHMS to include river water and groundwater use processes to better simulate the streamflow and assess the water resources in the

Yellow River Basin. To this end, the land surface, channel routing and groundwater models of AHMS are extended to account for river water and groundwater use in irrigation, and to include a scheme for estimating irrigated water requirement as proposed by Xu et al. (2019). These new developments lead to improved AHMS simulations, by reducing the errors associated with the underestimation of evaporation and the overestimation of runoff in the Yellow River Basin. We also show that the modelling of streamflow in the arid and semi-arid regions of the Yellow River Basin also improves upon consideration of irrigation.

2. Method

2.1. Introduction of the offline Atmospheric and Hydrological Modelling System (AHMS)

The Atmospheric and Hydrological Modelling System (AHMS) is a fully coupled atmospheric and hydrological modelling system (Jiang et al., 2020; Xia, 2019; Xia et al., 2022). Specifically, AHMS couples the Weather Research and Forecasting (WRF) modelling system (Skamarock & Klemp, 2008) with the physically-based distributed regional Hydrological Model System HMS (Yu et al., 2006) through the Noah-Multiparameterziation Land Surface Model (Noah-MP; Chen & Dudhia, 2001; Niu et al., 2011). Furthermore, the module in WRF-Hydro (Gochis et al., 2013) is employed for downscaling and upscaling of variables between the grids of land surface model and hydrological model.

AHMS can either be run online, i.e., coupled with the full WRF model for atmospheric dynamics, or offline – which is the situation adopted in the present study – by using prescribed near-surface atmospheric forcing variables. A schematic diagram identifying the main components of the online and offline AHMS simulations is displayed in Fig. 2. As shown in this figure, while the online AHMS can be employed to study the dynamic feedback between the atmosphere, surface and subsurface, the offline AHMS can be used to effectively calibrate and validate hydrological models.

Different from the previous work of Xia et al. (2022) combined the land surface hydrological model with the Global Crop Water Model (GCWM) to study hydrological processes in the water-rich areas of China, this study aims to develop an irrigation model that applies to arid and semi-arid regions. To this end, we extend AHMS to incorporate and modify a dynamic irrigation scheme (Xu et al., 2019) in Noah-MP, allowing us to quantify the dynamic irrigation water requirements of dryland crops based on the soil moisture deficit method. Furthermore, we incorporate the water uptake applicable to irrigation districts located in arid and semi-arid regions into the channel routing

model and groundwater model of HMS. Specifically, we develop a channel routing model that considers long-distance water supply processes in irrigation areas characteristic of arid and semi-arid regions, such as those in the Yellow River Basin.

A summary of the main components of the offline AHMS simulations applied in the present work is provided in the subsequent sections. Section 2.2 describes the hydrological models involved in the Noah-MP and HMS. Section 2.3 presents the irrigation scheme in AHMS. Figure 3 displays a schematic diagram of the hydrological cycle represented in AHMS and discussed in the following sections.

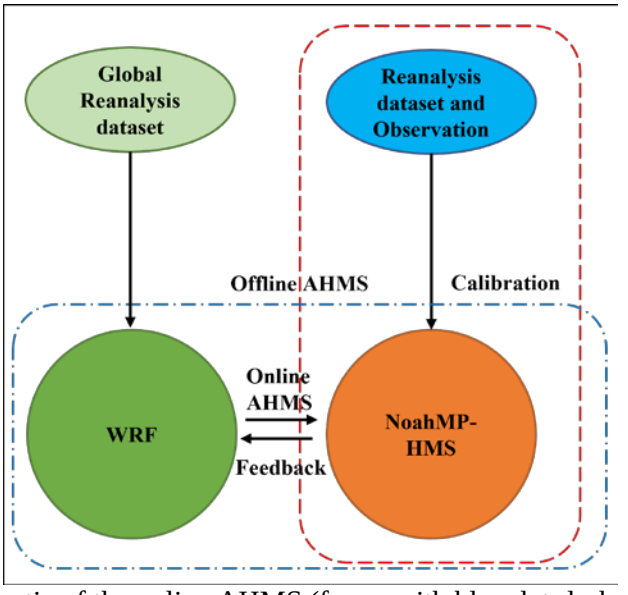

Figure 2: Simplified schematic of the online AHMS (frame with blue dot-dashed line) and offline AHMS (frame with red dashed line). Modified after Wagner et al. (2016b).

2.2. Hydrological modelling in Noah-MP and HMS

The land surface model Noah-MP is a single-column model that simulates the exchange of heat, moisture and momentum between the land surface and the atmosphere. The model provides a multi-parameterization framework for application in various land surface schemes (Chen & Dudhia, 2001; Niu et al., 2011). Furthermore, Noah-MP has been modified to be consistent with the HMS model, and Darcy's law boundary condition has been applied to simulate the moisture interactions between the unsaturated and saturated zones (Xia, 2019).

Moreover, the Hydrological Model System (HMS), developed for mesoscale and large-scale hydrological simulations by Yu et al. (2006), has been substantially improved in the framework of hydrological modelling (Xia, 2019). HMS is now applicable to simulate all main components involved in hydrological processes, including surface water flow, groundwater flow, and the

interaction flux between them. Specifically, the HMS model consists of three sub-models: a two-dimensional channel routing model (RT2D), a two-dimensional groundwater hydrological model (GW2D), and a groundwater and channel interaction model (GCI). These modules compute streamflow, groundwater flows from cell to cell and exchange with the stream, respectively.

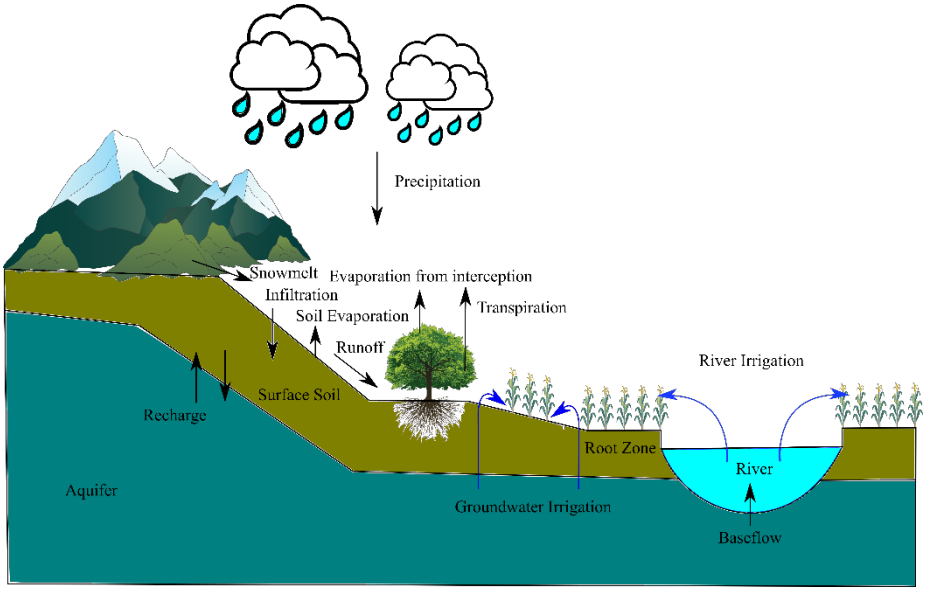

Figure 3: Sketch of the hydrologic cycle modelled in AHMS.

Noah-MP and HMS consider four surface soil layers with a total depth of 2 m and a single groundwater layer. The vertical movement of water in the surface soil is simulated by the Richard equation (see Section 2.2.1), while the horizontal movement of groundwater is modelled using the Boussinesq equation for unconfined conditions (see Section 2.2.2). The runoff rate is predicted based on the theory of infiltration-excess runoff (Horton runoff) (see Section S1 in the Supplementary Material) and saturation-excess runoff. Exchange water between surface soil and groundwater (drainage), river-groundwater and river-vadose zone (subsurface flow) are calculated according to Darcy's law (see Section S2 in the Supplementary Material). The flow routing is simulated by a diffusive wave model with the Manning equation (see Section 2.2.3), which can be used in low relief areas and account for backwater effects. Additional details about surface energy balances and vegetation dynamics of Noah-MP are described in Chen and Dudhia (2001) and Niu et al. (2011).

2.2.1 Vertical movement of soil water

The movement of soil water in the vertical direction is described by the Richards equation (Richards, 1931; Pachepsky et al., 2003)

$$\frac{\partial \theta}{\partial t} = \frac{\partial}{\partial z}\left[K\frac{\partial(\Psi + z)}{\partial z}\right] - S(z,t) \quad (1)$$

where θ is the volumetric soil water content [-], t is time [s], z is the height above the data in the soil column (positive upward) [m], K is the hydraulic conductivity [m s^{-1}], Ψ is the soil matric potential [m], and $S(z,t)$ is the soil moisture sink term (e.g., transpiration losses in the root zone). To solve Eq. (1), the following top boundary condition is considered

$$Q_{\mathrm{wat}} = P_{\mathrm{t}} + M - E_{\mathrm{g}} - R_{\mathrm{sf}} + Q_{\mathrm{irr}} \quad (2)$$

where Q_{wat} denotes the water input on the soil surface, P_{t} is the throughfall precipitation, M is the snow melt, E_{g} is the ground evaporation, R_{sf} is the surface runoff and Q_{irr} is the actual irrigated water including river irrigation and groundwater irrigation, which in the present study is added to the soil surface. Furthermore, we assume that the irrigation water is spread evenly and horizontally over the ground, while the actual irrigation input value on the soil surface is calculated from Eq. 8 (see Section 2.3).

2.2.2 2D single layer distributed groundwater model

The dynamics of the horizontal movement of groundwater are described by the following partial differential Boussinesq equation for unconfined conditions,

$$S_{\mathrm{p}}\frac{\partial h_{\mathrm{g}}}{\partial t} = \frac{\partial}{\partial x}\left(T_{\mathrm{g}}\frac{\partial h_{\mathrm{g}}}{\partial x}\right) + \frac{\partial}{\partial y}\left(T_{\mathrm{g}}\frac{\partial h_{\mathrm{g}}}{\partial y}\right) - Q_{\mathrm{net}}(x,y,t) \quad (3)$$

where T_{g} is the aquifer transmissivity [m^2 s^{-1}], S_{p} is the storage coefficient (porosity) [m^3 m^{-3}], Q_{net} [m s^{-1}] denotes the net contribution of sink and source terms, including the interaction flux between groundwater and unsaturated soil, the exchange of water between rivers and groundwater, and the extraction of groundwater from wells ($Q_{\mathrm{irr\_gw}}$).

2.2.3 Channel routing model

River and lake levels are represented by the prognostic variable h_{r}, which represents the thickness of surface water averaged over the grid cell. By combining the continuity of mass in the cell with the momentum equation for transport between cells, the rate of change of h_{r} can be written

as

$$A\frac{\partial h_{\mathrm{r}}}{\partial t}=\frac{\partial}{\partial x}\left(A_{\mathrm{c}}\frac{1}{n}R_{\mathrm{h}}^{2/3}\frac{\partial h_{\mathrm{r}}}{\partial x}\left|\frac{\partial h_{\mathrm{r}}}{\partial x}\right|^{-\frac{1}{2}}\right)+\frac{\partial}{\partial y}\left(A_{\mathrm{c}}\frac{1}{n}R_{\mathrm{h}}^{2/3}\frac{\partial h_{\mathrm{r}}}{\partial y}\left|\frac{\partial h_{\mathrm{r}}}{\partial y}\right|^{-\frac{1}{2}}\right)$$

$$+R_{\mathrm{sf}}-f_{\mathrm{w}}\left(C_{\mathrm{g}}+C_{\mathrm{u}}\right)-C_{\mathrm{l}}-Q_{\mathrm{irr\_sf}}(x,y,t) \quad (4)$$

where A is the river bed area of water in the river or lake [m^2], A_{c} is the cross-sectional area of water in the river or lake at cell boundaries [m^2], n is Manning's roughness coefficient [$\mathrm{s\ m}^{-1/3}$], and R_{sf} is the hydraulic radius [m], which is equivalent to $wd/(2d+w)$ for an open channel flow through a rectangular cross-section, with w and d denoting the width and depth of the river [m]. Furthermore, x and y denote the horizontal directions, and the water flow term between neighbouring grid cells is computed by considering all eight directions on the plane, including the diagonals. Specifically, for every grid cell in the square lattice constituting the simulation domain, Eq. (4) is solved by considering both nearest neighbouring cells in x and y directions, as well as in the diagonals (omitted from Eq. (4) for clarity). In addition, R_{sf} is the surface runoff [$\mathrm{m}^3\mathrm{s}^{-1}$], which encodes the infiltration-excess runoff (R_{ins}) and the saturation-excess runoff (R_{sat}), while f_{w} is the wetted surface fraction, which is set to 1 for lakes and to f_{b} for running rivers, with f_{b} denoting the fractional area of the river bed (computed following the method described next; see Eq. (S9) in the Supplementary Material). Moreover, C_{g}, C_{u} and C_{l} denote the values of water flux exchanged by the river with saturated soil, unsaturated soil and lake, respectively [$\mathrm{m}^3\ \mathrm{s}^{-1}$], while $Q_{\mathrm{irr\_sf}}$ is equal to the irrigated water from surface water, which has been added to the model in this study [$\mathrm{m}^3\ \mathrm{s}^{-1}$]. Water supply from the streams to the crops is modelled based on irrigation water demand predicted by the dynamic irrigation scheme in Noah-MP and constrained by the amount of available water in the stream (see Section 2.3 Eq. 9). More precisely, water is supplied to the crops located within the grid cells the streams flow across, as well as to the crops located in adjacent (off-stream) grid cells. The flow process is modelled here by means of the proximity grid search method, which considers the nearest neighbouring cells in x and y directions, as well as in the diagonals.

The Manning equation is used to estimate the average velocity $V_{x,y}$ [$\mathrm{m\ s}^{-1}$] of the river flow cross-section,

$$V_{x,y}=n^{-1}R_{\mathrm{h}}^{2/3}S_{\mathrm{f}}^{1/2} \quad (5)$$

where S_f is the friction slope [-]. To model $V_{x,y}$, we apply the diffusive wave equation by neglecting the local and convective acceleration terms and assuming that $S_f = S_{ws}$, where S_{ws} is the water surface slope [-]. Here, we follow Chow (2010), De Paiva et al., (2013) and Yamazaki et al., (2011), and assume that the Manning roughness coefficient is constant throughout the Yellow River Basin. The sensitivity of the AHMS to the Manning roughness coefficient n is discussed in Section S7 of the Supplementary Material.

2.3. Irrigation scheme in AHMS

The soil moisture deficit method in Noah-MP is employed to calculate the irrigation water requirements, i.e., when, where and how much to irrigate (Ozdogan et al., 2010; Xu et al., 2019). The equations for the integrated soil moisture availability (SMA) in root zones and irrigation water requirements (IWR) read,

$$\mathrm{SMA} = \frac{\mathrm{SM} - \mathrm{SM_{wlt}}}{\mathrm{SM_{ref}} - \mathrm{SM_{wlt}}} \tag{6}$$

$$\mathrm{IWR} = \min(\mathrm{SM_{ref}} - \mathrm{SM}\ , I_{\max}) \cdot F_{\mathrm{veg}} \cdot F_{\mathrm{crop}} \cdot (1.0 + F_{\mathrm{iloss}}) \tag{7}$$

where SM is the integrated soil moisture, and $\mathrm{SM_{ref}}$ and $\mathrm{SM_{wlt}}$ denote the integrated field capacity and wilting point in the root zones, respectively, $I_{\max}$ is the infiltration capacity, which is considered in the irrigation scheme in the present study (see Section S1 of the Supplementary Material), F_{veg} is the vegetation fraction, taken from the MODIS-based climatological dataset for the period from 2001 to 2012 (Broxton et al., 2014), and F_{crop} denotes the associated 500-m MODIS-based irrigation fraction (Ozdogan & Gutman, 2008). F_{iloss} is the fraction of flood irrigation loss which is set as 0.1 in this study.

The following irrigation conditions, based on irrigation fraction, rainfall, leaf area index, and soil water availability, are considered. Xu et al. (2019) reviewed the progress made in the control and optimization of various irrigation models and found that the following irrigation conditions, apply to a broad range of scales, from the field scale to the continental scale. The calibration and sensitivity of the AHMS to these irrigation parameters in the Yellow River Basin are described in Section S9 of the Supplementary Material.

(1) Cropland fraction: irrigation fraction is larger than the irrigation fraction threshold (IRR_FRAC), which is set to 0.25.
(2) Dry soil: soil moisture availability is less than the irrigation trigger criterion (IRR_MAD), which is set to 0.5.
(3) Weather: rainfall is less than the threshold rainfall rate (IR_RAIN), which is set to 1 mm/hr.
(4) Crop growing season: leaf area index is larger than the threshold leaf area index (IRR_LAI), which is set to 0.8.

The actual total irrigation water amount Q_{irr} is associated with both surface water and groundwater. However, this actual amount is limited by the availability of surface water in rivers and lakes. The following model applies,

$$Q_{\mathrm{irr}} = Q_{\mathrm{irr,sf}} + Q_{\mathrm{irr,gw}} \tag{8}$$

$$Q_{\mathrm{irr,sf}} = \min\left(\mathrm{IWR} * F_{\mathrm{irr,sw}}, W_{\mathrm{sf,avail}}\right) \tag{9}$$

$$Q_{\mathrm{irr,gw}} = \mathrm{IWR} * F_{\mathrm{irr,gw}} \tag{10}$$

where $Q_{\mathrm{irr,sf}}$ and $Q_{\mathrm{irr,gw}}$ denote the actual amounts of irrigation water from surface water (see Section 2.2.3, Eq. (4) in) and groundwater (see Section 2.2.2, Eq. (3)), respectively, while $F_{\mathrm{irr,sw}}$ and $F_{\mathrm{irr,gw}}$ are the corresponding area fractions of surface water (river) and groundwater irrigation, based on the "Global Map of Irrigation Areas" (Siebert et al., 2005). Moreover, $W_{\mathrm{sf,avail}}$ denotes the available surface water in the river or lake according to the channel routing model. Furthermore, we assume that groundwater is sufficient to meet irrigation demand.

3. Application to the Yellow River Basin

3.1. Study area

The Yellow River flows across Qinghai-Tibet Plateau, Inner Mongolia Plateau, Chinese Loess Plateau and Huanghuaihai Plain. The Yellow River Basin (Fig. 4) has an average temperature of -4° and annual precipitation of about 450 mm (references from the Yellow River Bulletin of Water Resources), which is unevenly distributed. The basin includes the Chinese Loess Plateau where most areas are arid or semi-arid regions. Moreover, the basin is characterized by a plateau and temperate climate and is strongly affected by the East Asian monsoon. The area of the upper and middle reaches above the Huayuankou station amounts to 730,036 km^2, thereby

accounting for 91.82% of the total basin area. Furthermore, the mean annual runoff at the Huayuankou station is 56.7 billion m^3, which corresponds to 96.42% of the total runoff of the Yellow River. The Yellow River located downstream of the Huayuankou station is an above-ground hanging river with a small catchment area, which covers about 3% of the Yellow River Basin (excluding the internal flow area of 42,000 km^2). Therefore, this study focuses on the upper reaches of the Huayuankou station, and the part of the Yellow River Basin referred to in this study corresponds to the upper reaches of the Huayuankou. Furthermore, these upper reaches of Huayuankou station are divided into four subbasins, namely TNH, TNH-LZ, LZ-TDG and TDG-HYK, which are associated with the four key hydrological stations in the region – including Tangnaihe, Lanzhou, Toudaoguai and Huayuankou.

3.2. Model input data

A Lambert conformal projection with standard parallel 38.3° N centred at 109.0° E is used to process input data at a resolution of 20 km for the Yellow River Basin.

3.2.1. Topography data

The high-resolution geographic digital elevation data set Multi-Error-Removed Improved-Terrain DEM (MERIT) with a 3sec resolution (Yamazaki et al., 2019) is used and upscaled to 20-km resolution by using an AHMS pre-processing program (Yu et al., 2006). In the upscaling process, the lower values are weighted more strongly to derive a consistent river network. The AHMS pre-processing program is combined with ArcSWAT to obtain the related hydrological data, i.e., river depth and width, water surface elevation, upstream area, and sub-basin area. Furthermore, the depth and width of the river channel are estimated from the empirical channel discharge-depth-width relationship (see Section S3 in the Supplementary Material), based on the theory of hydraulic geometry (Leopold & Maddock, 1953).

3.2.2. Subsurface data

The initial groundwater head is derived from the simulations using the global groundwater model (de Graaf et al., 2015). By using the China 1:4,000,000 Geology Dataset, the hydrogeologic parameters, including aquifer thickness, porosity and hydraulic conductivity of the aquifer are obtained correspondingly for each lithologic type with a lookup method (Yang et al., 2010).

3.2.3. Meteorological data

The forcing data applied in our simulations are obtained from the China Meteorological Forcing Dataset (CMFD) (He et al., 2020). These data include precipitation, near-surface air temperature, near-surface specific humidity, surface pressure, near-surface wind, surface downwelling shortwave and longwave radiation. CMFD is a high spatial-temporal resolution gridded near-surface meteorological dataset, which is specially designed for studies of land surface processes in China. This dataset was generated by combining remote sensing products, reanalysis datasets and in-situ observations from weather stations. Precipitation fields in CMFD were produced based on the assimilation of 753 weather stations from the China Meteorological Administration (CMA) and gridded background data including TRMM and GLDAS-NOAH.

3.2.4. Validation data

To calibrate and validate AHMS and the new irrigation model introduced here, we consider the observed daily water discharge dataset, publicly available from the National Earth System Science Data Center of China (http://loess.geodata.cn), and the estimated annual averages of surface water withdrawals for the period 1979-1988. The area associated with the referred dataset comprises the four main gauging stations TN (a), LZ (b), TDG (c) and HYK (d) of Yellow River Basin.

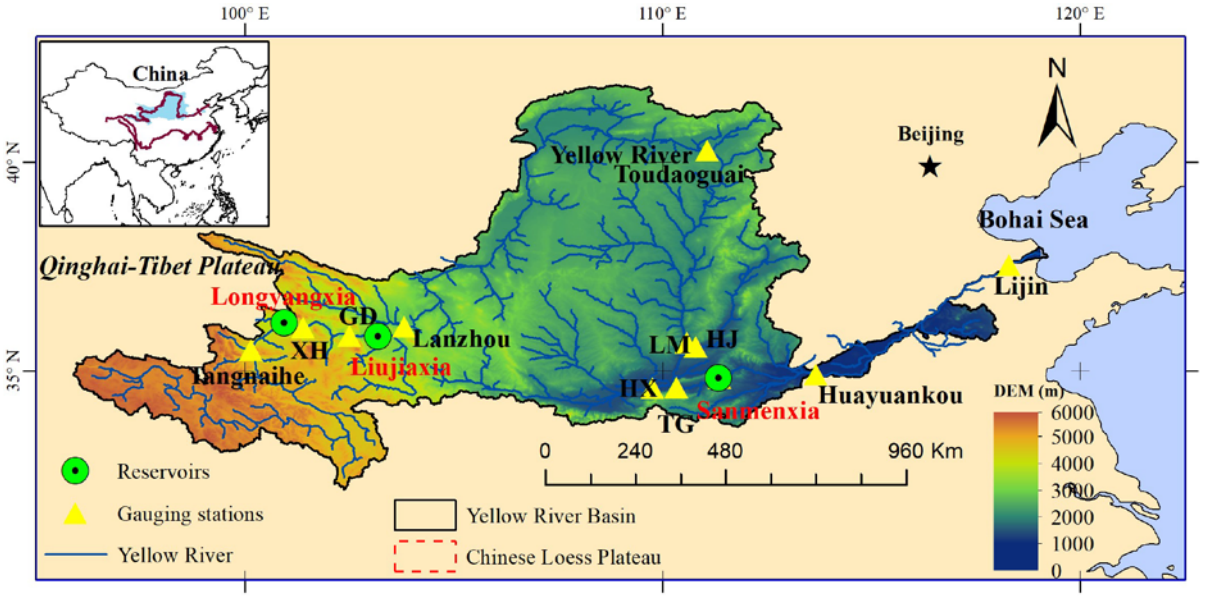

Figure 4: Location and topography of the Yellow River Basin. The map includes the Chinese Loess Plateau, the river network and the four main hydrological stations referred to in the main text, i.e., Tangnaihe (TNH), Lanzhou (LZ), Toudaoguai (TDG) and Huayuankou (HYK). The yellow triangles indicate these main

stations, as well as the stations of Guide (GD), Longmen (LM), Huaxian (HX) and Hejin (HJ), considered to evaluate the impacts of reservoirs on streamflow (see Section S5 in the Supplementary Material). The main reservoirs are indicated by the green cycles in the figure.

Specifically, due to the lack of data on direct statistical surface withdrawals from 1979 to 1987, we have estimated the corresponding annual averages of surface water withdrawals at the four gauging stations mentioned above, based on information available for five years from the Yellow River Bulletin of Water Resources (1999~2003) and Jia et al. (2006). According to the Yellow River Bulletin of Water Resources, in the period from 1999 to 2003, the percentage of whole basin average surface water withdrawals have been 0.6%, 9.12%, 45.38% and 17.18% at the four main gauging stations, respectively. Moreover, Jia et al. (2006) reported a value of approximately 24 km^3/yr for the average annual surface water withdrawals from 1980 to 1989. Therefore, the surface water use in the upper reaches of the TNH is negligible – the corresponding values are 2.34, 10.91 and 4.13 km^3/yr from 1979 to 1989 for the remaining three subbasins, respectively. Similarly, we have estimated the corresponding annual averages of surface water and groundwater withdrawals for irrigation from 1979 to 1989 in the area upstream of the HYK station mentioned above are 14.93 and 6.05 km^3/yr, respectively, for the period 1979 to 1989.

To validate our model prediction for evapotranspiration, we employ the Global Land Evaporation Amsterdam Model (GLEAM) v3.5 dataset (Martens et al., 2017), which has been acquired from satellite observations. Moreover, here we consider Gravity Recovery and Climate Experiment (GRACE) terrestrial water storage (TWS) data to evaluate modelled TWS on a regional scale. To this end, we have downloaded the latest GRACE products from the JPL-RL06M Mascon solutions (thereafter JPL-Mascon) (Wiese et al., 2018), provided by the Jet Propulsion Laboratory (JPL) at the 0.5-degree resolution and native resolution of JPL-RL06M of 3 degrees. JPL-Mascon has been pre-processed as follows. It is, firstly, masked by the land grid, and subsequently rescaled by using the scaling factors obtained by comparing the TWS of JPL-Mascon with the CLM4-based TWS provided by the GRACE website. Thereafter, the dataset is interpolated to a 0.25-degree grid (approximately 30 km on the equator).

Figure 5 shows that the TWS in the Yellow River Basin (upstream of HYK) is declining, with a linear trend of approximately 0.5 cm/yr from 2002 to 2022. Previous studies (e.g., Feng et al., 2013) have attributed this phenomenon to groundwater over-exploitation in north China. However, our current model does not account for the process of groundwater exploitation. Therefore, to apply the TWS dataset for the validation of our model, here we perform a detrend

analysis to remove the associated multi-year trend from the JPL-Mascon, thereby obtaining the orange curve in Fig. 5.

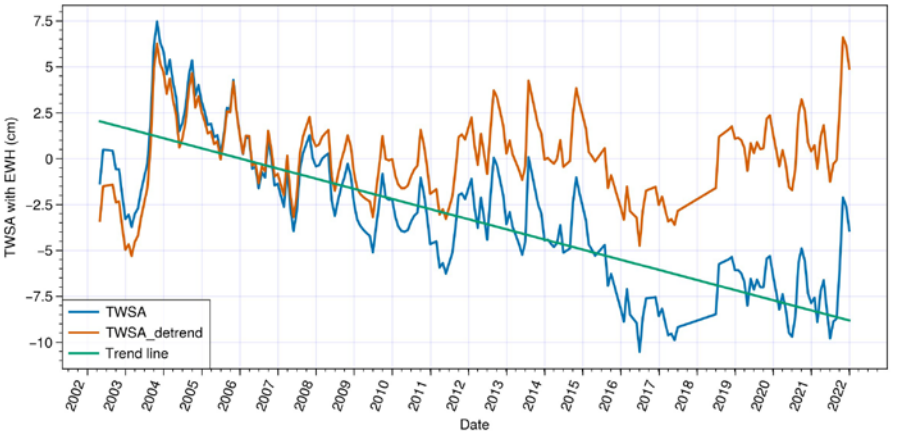

Figure 5: Monthly terrestrial water storage anomaly (TWSA) with equivalent water height (EWH) over 2002-2022 in the Yellow River Basin calculated from JPL-Mascon (solid blue line), detrend (solid yellow line), and linear trend line (green). The trend is about 0.5 cm per year.

3.3. Model setup and spin-up

Human interventions in the Yellow River Basin, including irrigation and dam construction, experienced substantial intensification during the last decades, with uncertain impacts on the evolution of the natural streamflow in the basin. Here, we focus on streamflow simulations from 1979 to 1988, for which both observed streamflow and meteorological data are available. To this end, model spin-up was conducted, firstly, over several decades to reach dynamic equilibrium, while the vegetation type and soil texture were assumed unchanged for the entire simulation period. The spatial and temporal resolutions of the land surface and hydrological models are 20 km and 60 minutes, respectively. Moreover, a summary of the physical and control parameterization schemes used in Noah-MP is listed in Tables S2 in Section S6 of the Supplementary Material.

3.4. Model performance evaluation indices

The agreement between the predicted and observed values of a given variable can be quantified using the percentage error (PE) and the square of the correlation coefficient according to Bravais-Pearson (r^2)

$$\mathrm{PE} = \frac{P - O}{O} \times 100\% \tag{11}$$

$$r^2 = \left(\frac{\sum_{i=1}^{N} (O^i - \bar{O})(P^i - \bar{P})}{\sqrt{\sum_{i=1}^{N} (O^i - \bar{O})^2} \sqrt{\sum_{i=1}^{N} (P^i - \bar{P})^2}} \right)^2 \quad (12)$$

where O and P denote observed and predicted values, N is the total number of observations, which are identified by the index i in the summation operator, and the upper horizontal bar indicates averaging over all data points in the time series. Furthermore, to quantify the agreement between predicted and observed streamflow, we employ the Nash–Sutcliffe model efficiency coefficient (NSE), defined through

$$\mathrm{NSE} = 1 - \frac{\sum_{i=1}^{N} (Q_s^i - Q_0^i)^2}{\sum_{i=1}^{N} (Q_0^i - \bar{Q}_0)^2} \quad (13)$$

where Q_s and Q_0 are the predicted and observed values of the streamflow, respectively, and $\bar{Q}_0$ denotes the average of the observed values. NSE ranges from minus infinity (poor fit) to 1.0 (perfect fit). In general, model prediction is considered to be satisfactory if $\mathrm{NSE} > 0.5$ (Moriasi et al., 2007).

3.5. Parameter calibration of hydrological model

The calibration of the hydrological model parameters often constitutes a laborious task due to a large number of parameters and a range of uncertainties. The sensitivity analysis presented in Section S7 in the Supplementary Material and Cuntz et al. (2016) indicates that the output fluxes, evapotranspiration, and runoff predicted from Noah-MP are sensitive to parameters related to both soil and vegetation characteristics. However, to calibrate average runoff in the land surface model for further studies, here we select the soil parameters (saturated hydraulic conductivity) that directly affect runoff generation and soil water budget. Moreover, the saturated hydraulic conductance of the riverbed (C_s) is calibrated against the observed baseflow.

However, according to Figure 1, the amount of artificial water withdrawals, including irrigation and domestic water, is very large and cannot be neglected in the computation of the regional water budget. Therefore, to calibrate the hydrological parameters, here we consider surface withdrawals (see Section 3.2.4) by comparing simulated total runoff with the sum of surface withdrawals and observed runoff. Four subbasins were selected to calibrate soil saturated hydraulic conductivity according to the climate, landscape conditions and human activity impact. The selected subbasins are the upstream areas of the Tangnaihai (TNH), Lanzhou (LZ), Toudaoguai (TDG) and Huayuankou

(HYK) gauges (see Fig. 4).

The calibrated hydrographs and the corresponding statistics are presented in Fig. 6. In this figure, the monthly streamflow series predicted with our simulations are compared with the observations at the four gauging stations from 1979 to 1988. The hydrograph is greatly improved by the calibration procedure and a reasonable agreement is found between these observations and the simulation results for upper stream stations (Tangnaihe and Lanzhou). Notably, the agreement is better at the upstream stations than at other stations in the midstream arid region. We thus conclude that the model must be improved to incorporate human activities in the midstream region, including the effect of river irrigation, which is the subject of Section 5.

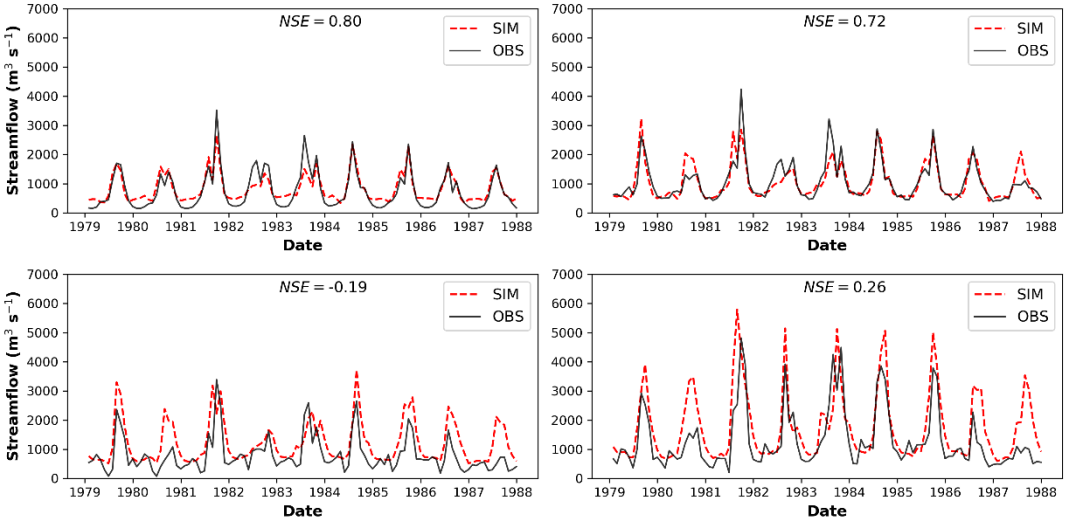

Figure 6: Predicted (dashed line) and observed (solid line) monthly streamflow from 1979 to 1987 at the hydrological stations: Tangnaihe (a), Lanzhou (b), Toudaoguai (c) and Huayuankou (d).

4. Evaluation and Discussion

The performance of the offline AHMS is evaluated in this section by means of terrestrial water budget analysis and by comparing the predicted and observed mean annual runoff and monthly streamflow, evapotranspiration and terrestrial water storage anomaly in the Yellow River Basin. Moreover, Section S8 in the Supplementary Material further describes the spatial distribution of eight hydrological variables including precipitation, evapotranspiration, runoff, streamflow, soil moisture, groundwater depth, surface runoff and subsurface runoff averaged annually from 1979 to 1988.

4.1. Terrestrial Water Budget

Water budget analysis offers a means to verify and evaluate hydrological models (De Paiva et al., 2013; Maurer et al., 2001). The corresponding mean annual terrestrial water budget for the Yellow River Basin is presented in Fig. 7a. As we can see from this figure, predicted and observed averaged annual precipitation values agree upon a percentage error (PE) of -2%, which gives us confidence that the input precipitation data from CMFD reanalysis products are reliable for the purpose of the present study. The deviation of the model water budget amounts to about 3% for precipitation, while the changes in total terrestrial water storage are about 3% of the precipitation. Furthermore, from the results obtained for the average annual evapotranspiration (PE is -5%) and runoff (PE is 35%), we conclude that the AHMS underestimates the evapotranspiration and overestimates the runoff if river irrigation is neglected.

Based on these findings, we further conclude that irrigation constitutes an essential component of the water balance in the Yellow River Basin, and must be incorporated into the AHMS model to improve the hydrological simulations. In Fig. 7b, the mean annual runoff over 1979-1988, as predicted from our simulations, is compared with the corresponding observation at four gauging stations over the same period, from 1979 to 1988. The APE values of runoff in the subbasins of TNH, TNH-LZ, LZ-TDG and TDG-HYK are 3%, 4%, -124% and 23%, respectively. Therefore, Figure 7b shows that the PE of the mean annual runoff is significant at the LZ-TDG subbasin. As mentioned before, the main source of this bias can be attributed to the river water used for irrigation in this region. Therefore, river water used for irrigation is an important component of the water balance, particularly in the semi-arid areas of the Yellow River Basin. Section 5 discusses the incorporation of river water taken for irrigation into AHMS simulations.

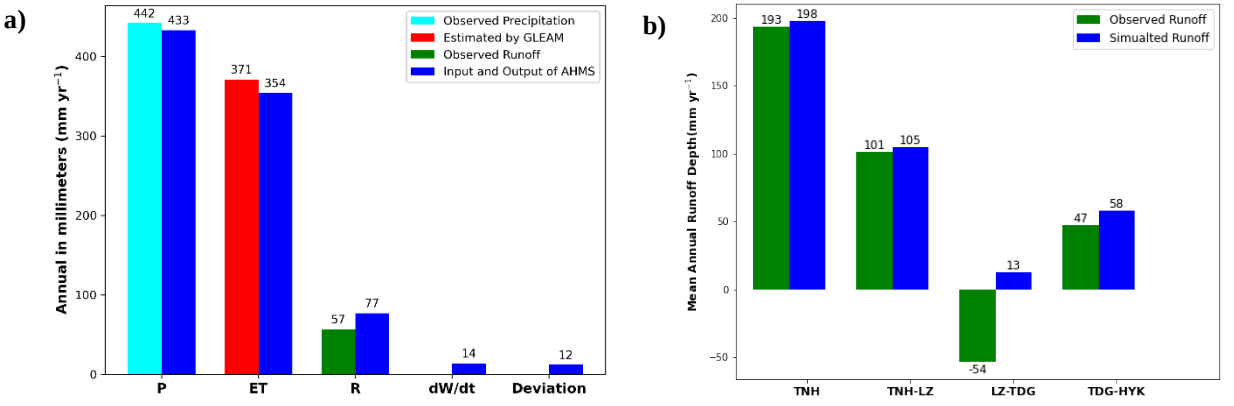

Figure 7: (a) Results from the water budget analysis. Displayed are the predicted and observed annual averaged precipitation, evapotranspiration and runoff over 1979-1988 in the Yellow River Basin. Annual observed precipitation is upscaled from daily precipitation data provided by the China Meteorological Administration, and GLEAM is the Global Land Evaporation Amsterdam Model, while the annual observed runoff is converted from daily streamflow at the gauging station (Huayuankou). **(b)** Predicted and

observed annual runoff averaged over 1979-1988 in the five subbasins of the Yellow River. Annual observed runoff is converted from the daily streamflow at gauging stations of Tangnaihe, Lanzhou, Toudaoguai and Huayuankou.

4.2. Evapotranspiration

Figure 8 displays monthly evapotranspiration at the Yellow River Basin estimated from the GLEAM, along with the corresponding prediction from the AHMS, for the period from 1980 to 1988. As shown in Fig. 8, the AHMS prediction agrees well with the GLEAM estimate, with the square of the correlation coefficient $r^2 \approx 0.98$, thus further corroborating the capability of our AHMS simulations to quantitatively describe long-term hydrological processes at the Yellow River Basin.

However, the AHMS slightly underestimates evapotranspiration, especially in the winter, notwithstanding the good agreement between the AHMS and GLEAM estimates with regard to the evaporation peaks. In particular, the evapotranspiration in January predicted using AHMS is clearly lower than the corresponding GLEAM estimate. Two factors could explain this underestimation. First, since groundwater provides the main source of water for evaporation during dry seasons, this underestimation of evapotranspiration could be associated with underestimated groundwater recharge in winter. Second, it has been noted in previous studies (Groisman & Legates, 1994; Yeh & Famiglietti, 2008) that measured precipitation from rain gauges have a systematic negative bias because of the local wind effect around rain gauges. This negative bias is greater in winter since snowflakes are more prone to wind deflections than raindrops. This underestimation of evapotranspiration may be thus caused by negative bias in the precipitation dataset, especially in winter.

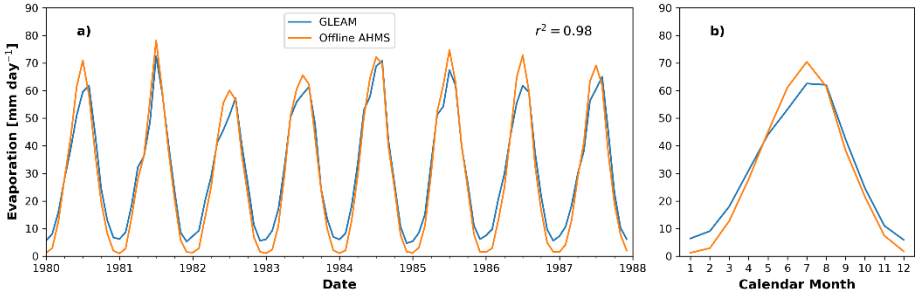

Figure 8: Comparison of evapotranspiration simulated by GLEAM and AHMS over 1980-1988 in the Yellow River Basin (a) monthly evapotranspiration (b) annual cycles of monthly evapotranspiration.

4.3. Terrestrial Water Storage

In Fig. 9, terrestrial water storage change (TWSC) predicted in numerical simulations using

AHMS and GLDAS is compared with the corresponding GRACE-based observation results. As can be now seen from Fig. 9, we find a good quantitative agreement (r^2=0.55) between the corresponding AHMS simulation predictions and their observation counterparts from the GRACE datasets. Moreover, the agreement of our AHMS simulation predictions compares reasonably well with corresponding predictions from the Global Land Data Assimilation System (GLDAS) results (r^2=0.56) too, as can be seen from Fig. 9. Therefore, AHMS represents the long-term, large-scale water cycle in the Yellow River basin with a good quantitative agreement with observations.

Furthermore, as shown in Fig. 9, our results indicate that terrestrial water storage changes (TWSC) in 2003-2004 have been much larger than in other years. This finding is consistent with the flooding that occurred in the middle and lower reaches of the Yellow River basin (Weihe River sub-basin) in August 2003. According to the 2003 Yellow River Water Resources Bulletin, the areal precipitation (555.6mm) of 2003 in the Yellow River Basin was 28.6% higher than the average areal precipitation (432mm) over the years (1956~2000). We thus attribute the higher TWS in the period from 2003 to 2004 (see Fig. 9) to the 2003 floods and the concatenated increase in infiltration and groundwater recharge. Our interpretation is in line with the association between precipitation and terrestrial water storage (Chen et al., 2010).

It should be noted that, while the TWSC in AHMS simulations is obtained by explicitly considering soil moisture, groundwater, and surface water of rivers and lakes, GLDAS (LSM-Noah) makes no explicit consideration of rivers and lakes in the simulations. This difference could explain the larger amplitude of the TWSC predicted using AHMS, compared to the corresponding GLDAS prediction. Therefore, we compare in Fig. 9 the GRACE-based monthly TWSC with the AHMS prediction TWSC of the surface water (ΔW_{sf}), soil moisture water (ΔW_{us}), and groundwater (ΔW_{gw}). Figure 10 indicates that changes in surface water, soil moisture and groundwater are associated with TWSC fluctuations of nearly the same magnitude.

It is interesting to note that surface water storage change including in rivers and lakes has been largely ignored in previous studies. For example, Cai et al. (2014) found, by applying the Noah-MP model for the Mississippi Basin, that soil moisture dominates the TWS anomalies, while groundwater constitutes the second component for this basin. However, consideration of surface water storage is indispensable for hydrological simulations of arid and semi-arid regions, such as the Yellow River Basin. Since the average annual precipitation in the Yellow River Basin is only about 450 mm, the upper reaches provide the main water resources for the arid and semi-arid middle and

lower reaches, i.e., terrestrial water storage in rivers plays a fundamental role in the Yellow River Basin and must be considered in the simulations.

We note that the TWSC should further depend on river width and depth, and on the area of the floodplains so the caveat must be added that some uncertainty exists about the values of these parameters, as discussed in the previous sections. Furthermore, the original AHMS models natural terrestrial water cycles, i.e., it does not consider the interference of human activities, such as reservoir storage and agricultural irrigation. The present work applies a coupled hydrological model of groundwater, soil moisture and channel routing model, thus making it possible to explicitly describe the contribution of each component to hydrological processes in the Yellow River Basin.

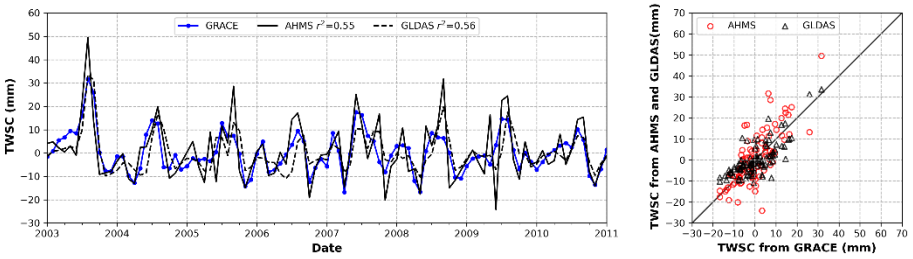

Figure 9: Monthly terrestrial water storage change (TWSC) with equivalent water height over 2003-2011 in the Yellow River Basin calculated from GRACE dataset observation: JPL-mascono (solid blue line with circles), the offline AHMS simulation (solid black line; red circle) and the Global Land Data Assimilation System (GLDAS) (dash black line and black rectangle).

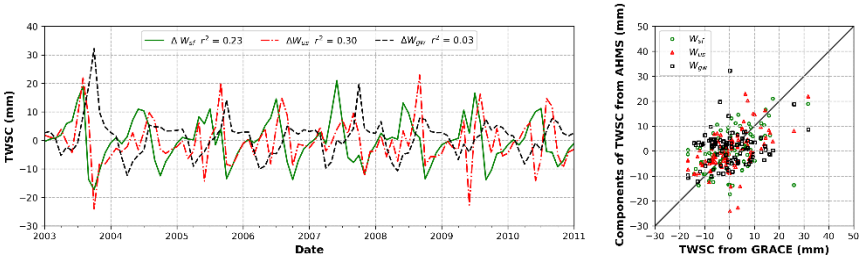

Figure 10: Comparison of the monthly GRCAE-based TWSC with components of AHMS simulation including changes of surface water; (ΔW_{sf}; green line and circles), soil moisture water (ΔW_{us}; red dash line and triangles) and groundwater (ΔW_{gw}; black dash line and rectangles) over 2003-2011 in the Yellow River Basin.

5. Irrigation Impact on the Runoff, Evapotranspiration and Streamflow in the Yellow River Basin

Irrigation water is an important component of the water balance in the arid and semi-arid areas and strongly affects streamflow in the Yellow River Basin. As can be seen from Fig 7b, the Lanzhou-Tangnaihe (LZ-TDG) subbasin is a net water consumption region. However, the current operational version of the AHMS does not account for the effect of water taken from the Yellow River for

irrigation. We thus attribute the discrepancy between predicted and observed average annual runoff at the LZ-TDG station (see Fig. 7b; the predicted average annual runoff is positive while the observed one is negative) to the lack of a representation of irrigation water in the model.

Here we extend the land surface, channel routing and groundwater models of AHMS to include the effect of water taken from the Yellow River for irrigation (Q_{irr} in Eq. (2), $Q_{\mathrm{irr\_gw}}$ in Eq. (3) and $Q_{\mathrm{irr\_sf}}$ in Eq. (4)). To this end, we combine the land surface model Noah-MP in the AHMS with a dynamic irrigation scheme (Xu et al., 2019) to quantify the dynamic water requirements for irrigation which is based on soil moisture deficit. Furthermore, the actual river irrigation is further constrained by the amount of available water, as well as by the fraction of river water within the total irrigation based on the statistics of irrigation facilities (see Section 2.3). As described in Section 2.3, five parameters related to the irrigation model are considered. The calibration and sensitivity analysis of these parameters are shown in Section S9 of the Supplementary Material. In the following paragraphs, we discuss the results obtained from AHMS, using the calibrated parameter values in our irrigation model.

Table 1 Comparison of statistical and simulated areal average annual irrigation in the Yellow River Basin from 1979 to 1987 (mm/yr)

Period	River irrigation			Groundwater irrigation			Total irrigation		
	Statistics	Simulation	PE (%)	Statistics	Simulation	PE (%)	Statistics	Simulation	PE (%)
1979~1987	20.5	14.9	-27.3	8.3	11.2	35.0	28.8	26.1	9.4

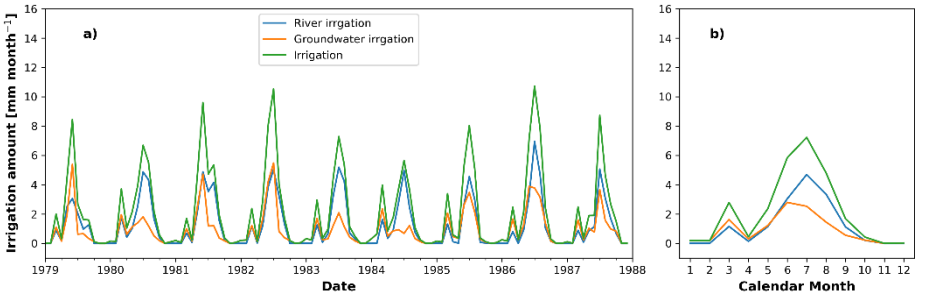

Figure 11: (a) Monthly and (b) annual averaged cycles of total irrigation amount (green line) in the Yellow River Basin (upper reaches of Huayuankou station) for the period of 1978-1988, including river irrigation (blue line) and groundwater irrigation (orange line).

To validate and evaluate the irrigation model, we compare the simulated areal average annual irrigation amount with regional statistics (see Section 3.2.4) from 1979 to 1988. As shown in Table 1, the model simulates the total areal average annual irrigation well, but the model underestimates river irrigation and overestimates groundwater irrigation. Moreover, we perform the sensitivity

analysis of the irrigation amount including river irrigation and groundwater irrigation and the average monthly streamflow at the outlet of the Yellow River Basin (HYK) to the irrigation parameters (see Table S4 in Section S9 of the Supplementary Material). We find that the model greatly underestimates the amount of river irrigation in the Yellow River Basin if the long-distance transfer of water from the river to the irrigation area is not considered (see Table S5 in Section S9 of the Supplementary Material). Furthermore, Figure 11 represents the monthly and annual averaged cycles of actual irrigation amount including river irrigation and groundwater irrigation in the Yellow River Basin. The temporal distribution of irrigation water consumption indicates that the maximum water consumption rate occurs in June, while during the winter the basin relies heavily on groundwater irrigation.

Figure 12a displays the annual averaged precipitation, evapotranspiration and runoff for the period 1979-1988, obtained from the simulation under consideration of irrigation in the Yellow River Basin, along with the corresponding observations. Compared to the results displayed in Fig. 7 (no irrigation), the percentage error (PE) of evapotranspiration and runoff changed from -5% to -2% and from 35% to 9%, respectively. Moreover, the annual average runoff obtained from the model with irrigation is compared against the observed value in Fig. 12b. As can be seen by comparing Fig. 12b with Fig. 7b (no irrigation), the incorporation of irrigation substantially improved the model predictions. In particular, in Fig. 12b, the negative average annual runoff at the LZ-TDG subbasin is accurately reproduced by the model, as a result of considering irrigation.

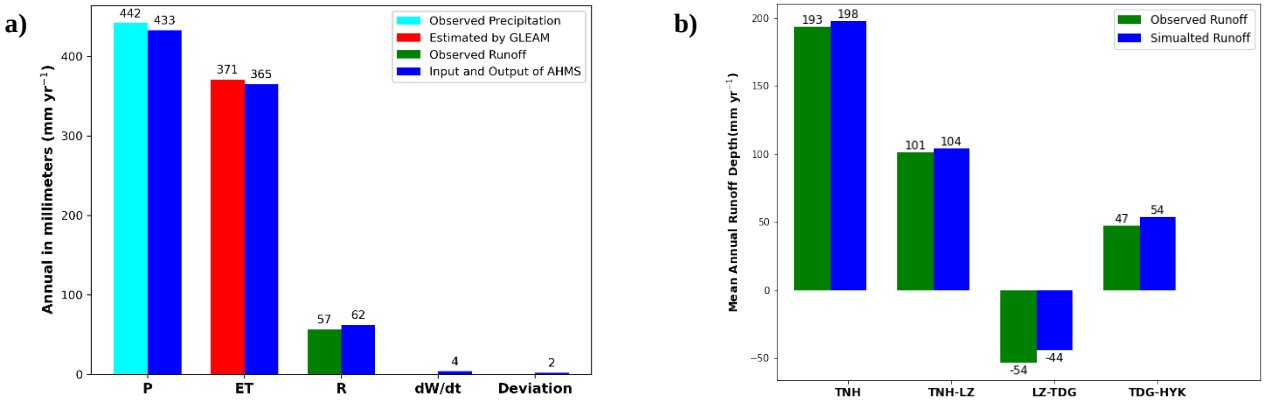

Figure 12: As in Figure 7, but now considering irrigation in the AHMS simulation.

Furthermore, we compare the GLEAM estimate for the evapotranspiration in the Yellow River Basin in the period of 1980-1988 with the corresponding predictions from the AHMS simulation, obtained under consideration of taking water from the river for irrigation. The results for the Yellow River Basin are shown in Fig. 13. Since microwave observations of surface soil moisture are

assimilated into the GLEAM soil profile to correct for forcing errors in GLEAM (Martens et al., 2016), the evapotranspiration estimated by GLEAM should be able to reflect the effects of irrigation. However, the incorporation of irrigation into the model does not improve the agreement between GLEAM estimates and AHMS predictions of evapotranspiration – the coefficient of determination (r^2) decreased slightly from 0.98 to 0.97 upon including irrigation. This behavior can be understood by noting that the original AHMS simulation without irrigation already overestimates evapotranspiration in the summer (see Section 4.2). We find that this overestimation is slightly enhanced by considering irrigation, as indicated by the respective square of the correlation coefficient. Our findings clearly show, thus, that evapotranspiration is overestimated by AHMS in the summer and underestimated in the winter, and that this behaviour is not caused by our irrigation model. Therefore, future research should focus on elucidating this behaviour to improve the overall accuracy of AHMS, and its applicability to the arid and semi-arid regions of the Yellow River Basin.

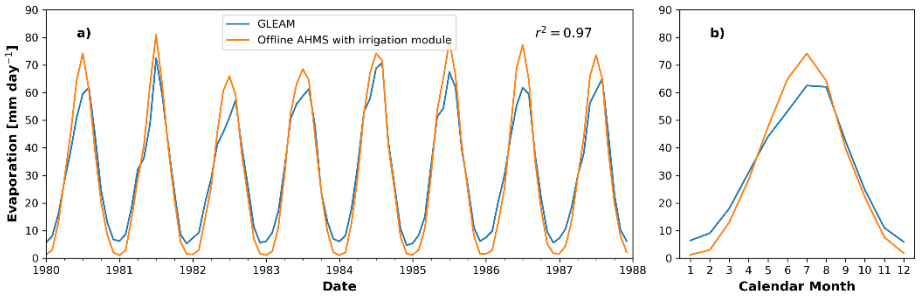

Figure 13: As in Figure 8, but now considering irrigation in the AHMS simulation (orange line).

Next, we investigate the effect of irrigation on the changes in terrestrial water storage change (TWSC). Figure 14a and Figure 14b compare TWSC computed from the GRACE-based monthly observations with the prediction from the AHMS simulation, considering the different model components affected by water taken from rivers and groundwater for irrigation. We find that the agreement of TWSC between AHMS simulations and GRACE observations improved when irrigation was taken into account, with the respective r^2 values changing from 0.55 (without irrigation) to 0.57 (with irrigation). In particular, the consistency between the GRACE-based TWSC and the surface water changes (ΔW_{sf}) improved significantly due to the inclusion of irrigation, with the associated r^2 increasing from 0.23 to 0.39. Moreover, the difference between the GRACE-based TWSC and the soil moisture water changes (ΔW_{us}) was reduced moderately, with the associated r^2 increasing from 0.30 to 0.36. However, there are no significant improvements in the comparison between the GRACE-based TWSC and groundwater changes (ΔW_{gw}).

Figure 15 compares our model predictions with observations of the monthly (Figure 15a) and averaged monthly (Figure 15b) streamflow at the outlet of the middle reaches of the Yellow River Basin (Huayuankou station) for 1979-1988. In Figs. 15a and 15b, the comparison is made both with and without water taken from the river for irrigation in the large irrigation districts – including the Hetao Plateau and Ningxia agriculture area. The results displayed in Figs. 15a and 15b show that AHMS predictions of streamflow agree more closely with observation data when irrigation is considered in the simulation.

Consideration of irrigation has led to a reduction in the systematic errors associated with the streamflow simulations. As can be seen in Fig. 15b, the integration error has been reduced from zone to zone in the Yellow River Basin. More precisely, the Nash-Sutcliffe model efficiency (NSE) changed from 0.26 (without irrigation) to 0.55 (with irrigation) for the monthly streamflow changes, and from 0.27 (without irrigation) to 0.82 with irrigation) for the mean monthly streamflow changes. Model performance improves significantly (see area A in Fig. 15b) with consideration of irrigation. However, various sources for the remaining error associated with the area in Fig. 15 should be elucidated in future work. To address the remaining error in streamflow (see area B in Fig. 15b), the influence of industrial and domestic water use, as well as dam regulations, should be also included in future modelling to improve the model of water use in AHMS.

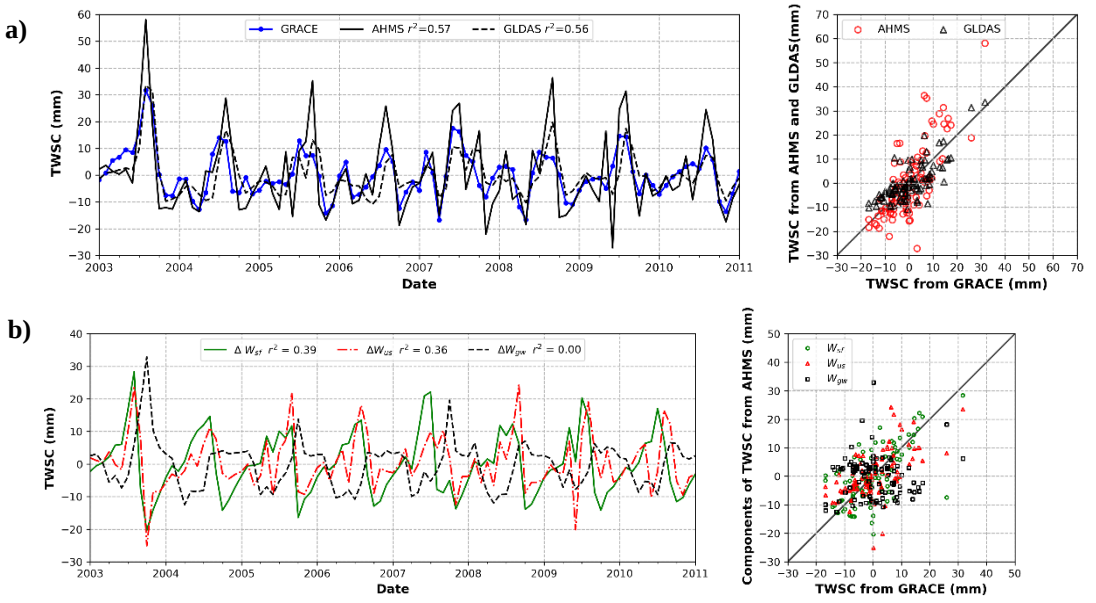

Figure 14: As in Figure 9 (a) and Figure 10, but now considering irrigation in the AHMS simulation.

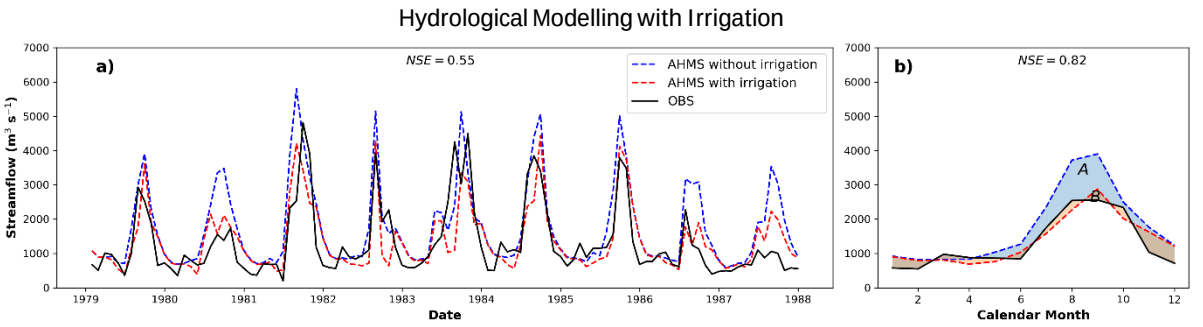

Figure 15: Comparison of (a) monthly and (b) averaged annual cycles of predicted (dashed lines), which is with (red) and without (blue) consideration of irrigation, and observed (solid line) streamflow at outlet of middle reaches of Yellow River Basin (Huayuankou station) for the period of 1979-1988.

Our model has provided insights into the relevance of irrigation for hydrological processes throughout the Yellow River Basin. As can be seen from Figs. 6 and 7a, a good agreement between predicted and observed runoff and streamflow in the basin's upstream region (Tangnaihe and Lanzhou stations) could be obtained in simulations without irrigation, after calibration of the soil hydraulic conductivity. However, the mere calibration of this parameter could not yield a satisfactory comparison between corresponding observations and model results in the midstream area (Huayuankou station). Good quantitative agreement including the midstream area could be only found after the incorporation of our irrigation module – see Figures 12b and 15. Therefore, our model results clearly show that irrigation plays a major role in hydrological processes in the midstream area of the Yellow River Basin (Huayuankou station), which is characterized by an arid and semi-arid climate. Our irrigation module should be thus considered in future regional hydrological modelling of arid and semi-arid hydrological basins.

6. Conclusion and Outlook

In the present work, a regional model for long-term, large-scale hydrological processes under consideration of irrigation in the arid and semi-arid regions (AHMS-IRRIG) has been presented. The model (AHMS-IRRIG) combines the land surface model, the flow routing model and the groundwater model of the Atmospheric and Hydrological Modelling System (AHMS) with a modified irrigation scheme (Xu et al., 2019) to quantify the dynamic irrigation amount in arid and semi-arid basins. Specifically, this study developed a dynamic irrigation model based on the soil moisture deficit method and constrained by water availability for the arid and semi-arid regions. Moreover, the channel routing model and groundwater model of the AHMS has been modified here to incorporate the water uptake applicable to the long-distance water supply to irrigation districts in

an arid and semi-arid basin. Furthermore, the actual amount of irrigation is therefore constrained by the water availability estimated with the flow routing, as well as the irrigation fractions of surface water and groundwater based on the "Global Map of Irrigation Areas". AHMS-IRRIG has been then applied to hydrological simulations of the Yellow River Basin for the period 1979-2011 to assess the impact of irrigation on the land surface processes in the basin's arid and semi-arid areas.

To this end, AHMS has been first calibrated and evaluated for the Yellow River Basin by means of a parameter sensitivity analysis and a terrestrial water budget analysis, and through a comparison of model predictions for the mean annual runoff, monthly streamflow, evapotranspiration and terrestrial water storage anomaly with corresponding observation data, both from in-situ and remote sensing datasets. Furthermore, to account for water consumption in the Yellow River, the land surface, channel routing and groundwater models have been extended to account for water taken from the river for irrigation. The irrigation water demand calculated by the dynamic irrigation scheme in Noah-MP was added to the sink term and further constrained by water availability in the flow routing and groundwater model, and then actual irrigation water is distributed evenly and horizontally over the ground in the land surface model.

By incorporating the irrigation module into the simulation, a more realistic hydrologic response near the outlet of the Yellow River Basin could be obtained. Moreover, a quantitative agreement was found between the predicted discharge at the upstream gauging stations, namely, Tangnaihe and Lanzhou, and the corresponding observation data. A reasonable agreement between model TWSC and observations from GRACE was also found. Monthly evapotranspiration estimated by GLEAM and the one modelled by AHMS were found to agree well with each other, with the square of correlation coefficient (r^2) of about 0.98. Our results thus demonstrate the capability of AHMS of reproducing long-term hydrological processes in the Yellow River Basin, provided water taken from irrigation is considered in the simulation.

Therefore, the main novelties of our model development and application can be summarized as follows:

1) The development of an irrigation model that considers the long-distance water transfer off-stream from the river to irrigation districts – is fully neglected by previous irrigation models. With our model, the actual irrigation amount is explicitly computed using the soil moisture deficit method and constrained by the water availability estimated with the flow routing, as well as the irrigation fractions of surface water and groundwater based on the "Global Map of Irrigation Areas";

2) The development of a regional hydrological model that is applicable to arid and semi-arid regions, through the incorporation of irrigation sink and source terms into the channel routing and groundwater models;
3) The incorporation of the advanced Earth gravity satellite (GRACE) dataset for the verification of our hydrological model and the assessment of irrigation impacts on hydrological processes in the arid and semi-arid environments of the Yellow River Basin.

Therefore, the future application of our model has the potential to substantially improve the quantitative assessment of the irrigation impacts on hydrological processes in arid and semi-arid areas, by incorporating our irrigation module into the regional AHMS simulation. Furthermore, our model shall provide a helpful tool in the study of feedback effects between irrigation, rainfall and temperature in arid and semi-arid regions, by means of (online) numerical simulations coupled with the Weather Research Forecasting (WRF) modelling system. Moreover, the hydrological model extended here to incorporate our irrigation module shall also find application in the study of irrigation effects on local environmental processes under consideration of changes in climate and land use type.

However, the current version of AHMS needs to be improved in different ways to more accurately represent hydrological processes in the semi-arid and arid areas of the Yellow River Basin. In the present study, only soil parameters were calibrated from the land surface model. The incorporation of vegetation parameters into the calibration of the numerical simulations would constitute one important model extension in future work. Additional measurement data of river and floodplain geometry for the channel routing model of the AHMS would also improve the prediction of flood timing and peak. Furthermore, the incorporation of various anthropogenic influences, such as damming or groundwater supplies for irrigation, and the inclusion of a dynamic crop and damming model into AHMS constitutes an open modelling task, which will be important to improve the quantitative assessment of the hydrological processes in future work.

Overall, the extension of AHMS presented here led to a more reliable model for predicting runoff and streamflow in arid and semi-arid regions, such as the Yellow River Basin. The progress achieved in the present work shall pave the way toward a wider model application of AHMS at the regional scale over the Yellow River Basin and other hydrological systems in future work, including a broader range of climatic and environmental conditions, and anthropogenic influences.

Software availability

Software name: AHMS-IRRIG

Developer: Cong Jiang, Qian Xia

Hardware requirements: PC, HPC

System requirements: Linux

Program language: Fortran

Availability: https://github.com/JiangCong1990/AHMS-IRRIG

License: Free and open source

Documentation: README and guided example in Github repository

Acknowledgement

This research was supported by the German Research Foundation (DFG) through the Heisenberg Programme "Multiscale Simulation of Earth Surface Processes", project number 434377576. The China Meteorological Forcing Dataset (CMFD) is provided by National Tibetan Plateau Data Center (http://data.tpdc.ac.cn). Daily Yellow River discharge data is supported by "Loess Plateau SubCenter, National Earth System Science Data Center, National Science & Technology Infrastructure of China. (http://loess.geodata.cn)". The data used in this study can be found online (https://github.com/JiangCong1990/AHMS-IRRIG). The authors declare that they have no conflict of interest.

CRediT authorship contribution statement

Cong Jiang: Formal analysis, Methodology, Software, Validation, Writing - Original Draft, Writing - Review & Editing. **Eric J. R. Parteli:** Conceptualization, Supervision, Funding acquisition, Writing - Review & Editing. **Qian Xia:** Software. **Xin Yin:** Investigation, Visualization. **Yaping Shao:** Conceptualization, Supervision, Funding acquisition, Writing – Review & Editing, Resources.

References

Broxton, P. D., Zeng, X., Scheftic, W., & Troch, P. A. (2014). A MODIS-based global 1-km maximum green vegetation fraction dataset. *Journal of Applied Meteorology and Climatology*, *53*(8), 1996–2004.

Chen, F., & Dudhia, J. (2001). Coupling and advanced land surface-hydrology model with the Penn State-NCAR MM5 modeling system. Part I: Model implementation and sensitivity. *Monthly Weather Review*, *129*(4), 569–585. https://doi.org/10.1175/1520-0493(2001)129<0569:CAALSH>2.0.CO;2

Chen, J. L., Wilson, C. R., & Tapley, B. D. (2010). The 2009 exceptional Amazon flood and interannual terrestrial water storage change observed by GRACE. *Water Resources Research*, *46*(12).

Chow, V. Te. (2010). *Applied Hydrology*. Tata McGraw-Hill Education.

Cong, Z., Yang, D., Gao, B., Yang, H., & Hu, H. (2009). Hydrological trend analysis in the Yellow River Basin using a distributed hydrological model. *Water Resources Research*, *45*(7).

de Graaf, I. E. M. de, Sutanudjaja, E. H., Van Beek, L. P. H., & Bierkens, M. F. P. (2015). A high-resolution global-scale groundwater model. *Hydrology and Earth System Sciences*, *19*(2), 823–837.

De Paiva, R. C. D., Buarque, D. C., Collischonn, W., Bonnet, M.-P., Frappart, F., Calmant, S., & Bulhões Mendes, C. A. (2013). Large-scale hydrologic and hydrodynamic modeling of the Amazon River Basin. *Water Resources Research*, *49*(3), 1226–1243.

Feng, W., Zhong, M., Lemoine, J.-M., Biancale, R., Hsu, H.-T., & Xia, J. (2013). Evaluation of groundwater depletion in North China using the Gravity Recovery and Climate Experiment (GRACE) data and ground-based measurements. *Water Resources Research*, *49*(4), 2110–2118.

Gochis, D. J., Yu, W., & Yates, D. N. (2013). The WRF-Hydro model technical description and user's guide, Version 1.0. *Http://Www.Ral.Ucar.Edu/Projects/Wrf_hydro/*, 1–120.

Groisman, P. Y., & Legates, D. R. (1994). The accuracy of United States precipitation data. *Bulletin of the American Meteorological Society*, *75*(2), 215–228.

He, J., Yang, K., Tang, W., Lu, H., Qin, J., Chen, Y., & Li, X. (2020). The first high-resolution meteorological forcing dataset for land process studies over China. *Scientific Data*, *7*(1), 1–11. https://doi.org/10.1038/s41597-020-0369-y

Jia, Y., Wang, H., Zhou, Z., Qiu, Y., Luo, X., Wang, J., Yan, D., & Qin, D. (2006). Development of the WEP-L distributed hydrological model and dynamic assessment of water resources in the Yellow River Basin. *Journal of Hydrology*, *331*(3–4), 606–629.

Jiang, C., Parteli, E. J. R., & Shao, Y. (2020). Application of a Coupled Atmospheric and Hydrological Modelling System (AHMS) to the Yellow River Basin, China. *EGU General Assembly Conference Abstracts*, 5197.

Leopold, L. B., & Maddock, T. (1953). *The hydraulic geometry of stream channels and some physiographic implications* (Vol. 252). US Government Printing Office.

Martens, B., Miralles, D. G., Lievens, H., Schalie, R. van der, De Jeu, R. A. M., Fernández-Prieto, D., Beck, H. E., Dorigo, W. A., & Verhoest, N. E. C. (2017). GLEAM v3: Satellite-based land evaporation and root-zone soil moisture. *Geoscientific Model Development*, *10*(5), 1903–1925.

Maurer, E. P., O'Donnell, G. M., Lettenmaier, D. P., & Roads, J. O. (2001). Evaluation of the land surface water budget in NCEP/NCAR and NCEP/DOE reanalyses using an off-line hydrologic model. *Journal of Geophysical Research: Atmospheres*, *106*(D16), 17841–17862.

Maxwell, R. M., Chow, F. K., & Kollet, S. J. (2007). The groundwater-land-surface-atmosphere connection: Soil moisture effects on the atmospheric boundary layer in fully-coupled simulations. *Advances in Water Resources*, *30*(12), 2447–2466. https://doi.org/10.1016/j.advwatres.2007.05.018

Maxwell, R. M., Lundquist, J. K., Mirocha, J. D., Smith, S. G., Woodward, C. S., & Tompson, A. F. B. (2011). Development of a coupled groundwater-atmosphere model. *Monthly Weather Review*, *139*(1), 96–116. https://doi.org/10.1175/2010MWR3392.1

Moriasi, D. N., Arnold, J. G., Van Liew, M. W., Bingner, R. L., Harmel, R. D., & Veith, T. L. (2007). Model evaluation guidelines for systematic quantification of accuracy in watershed

simulations. *Transactions of the ASABE*, *50*(3), 885–900.
Niu, G. Y., Yang, Z. L., Mitchell, K. E., Chen, F., Ek, M. B., Barlage, M., Kumar, A., Manning, K., Niyogi, D., Rosero, E., & others. (2011). The community Noah land surface model with multiparameterization options (Noah-MP): 1. Model description and evaluation with local-scale measurements. *Journal of Geophysical Research: Atmospheres*, *116*(D12).
Ozdogan, M., & Gutman, G. (2008). A new methodology to map irrigated areas using multi-temporal MODIS and ancillary data: An application example in the continental US. *Remote Sensing of Environment*, *112*(9), 3520–3537.
Ozdogan, M., Rodell, M., Beaudoing, H. K., & Toll, D. L. (2010). Simulating the effects of irrigation over the United States in a land surface model based on satellite-derived agricultural data. *Journal of Hydrometeorology*, *11*(1), 171–184.
Pilgrim, D. H., Chapman, T. G., & Doran, D. G. (1988). Problems of rainfall-runoff modelling in arid and semiarid regions. *Hydrological Sciences Journal*, *33*(4), 379–400.
Rafiei-Sardooi, E., Azareh, A., Shooshtari, S. J., & Parteli, E. J. R. (2022). Long-term assessment of land-use and climate change on water scarcity in an arid basin in Iran. *Ecological Modelling*, *467*, 109934.
Shrestha, P., Sulis, M., Masbou, M., Kollet, S., & Simmer, C. (2014). A scale-consistent terrestrial systems modeling platform based on COSMO, CLM, and ParFlow. *Monthly Weather Review*, *142*(9), 3466–3483.
Siebert, S., Döll, P., Hoogeveen, J., Faures, J.-M., Frenken, K., & Feick, S. (2005). Development and validation of the global map of irrigation areas. *Hydrology and Earth System Sciences*, *9*(5), 535–547.
Skamarock, W. C., & Klemp, J. B. (2008). A time-split nonhydrostatic atmospheric model for weather research and forecasting applications. *Journal of Computational Physics*, *227*(7), 3465–3485.
Wagner, S., Fersch, B., Yuan, F., Yu, Z., & Kunstmann, H. (2016). *WRF-HMS , a fully-coupled regional atmospheric-hydrological modeling system for long-term scale applications*. *18*(EUG2016), 12321.
Wiese, D. N., Yuan, D. N., Boening, C., Landerer, F. W., & Watkins, M. M. (2018). JPL GRACE mascon ocean, ice, and hydrology equivalent water height release 06 coastal resolution improvement (CRI) filtered version 1.0. *DAAC: Pasadena, CA, USA*.
Wilby, R., Greenfield, B., & Glenny, C. (1994). A coupled synoptic-hydrological model for climate change impact assessment. *Journal of Hydrology*, *153*(1–4), 265–290.
Xia, Q. (2019). *Development and Application of a Coupled Atmospheric and Hydrological Modelling System*. 1–125.
Xia, Q., Liu, P., Fan, Y., Cheng, L., An, R., Xie, K., & Zhou, L. (2022). *Representing Irrigation Processes in the Land Surface- Hydrological Model and a Case Study in the Yangtze River*.
Xu, X., Chen, F., Barlage, M., Gochis, D., Miao, S., & Shen, S. (2019). Lessons learned from modeling irrigation from field to regional scales. *Journal of Advances in Modeling Earth Systems*, *11*(8), 2428–2448.
Yamazaki, D., Ikeshima, D., Sosa, J., Bates, P. D., Allen, G. H., & Pavelsky, T. M. (2019). MERIT Hydro: A high-resolution global hydrography map based on latest topography dataset. *Water Resources Research*, *55*(6), 5053–5073.
Yamazaki, D., Kanae, S., Kim, H., & Oki, T. (2011). A physically based description of floodplain inundation dynamics in a global river routing model. *Water Resources Research*, *47*(4).
Yang, C., Lin, Z., Yu, Z., Hao, Z., & Liu, S. (2010). Analysis and simulation of human activity impact on streamflow in the Huaihe River Basin with a large-scale hydrologic model. *Journal*

of Hydrometeorology, *11*(3), 810–821.
Yeh, P. J.-F., & Famiglietti, J. S. (2008). Regional terrestrial water storage change and evapotranspiration from terrestrial and atmospheric water balance computations. *Journal of Geophysical Research: Atmospheres*, *113*(D9).
Yin, Z., Ottle, C., Ciais, P., Zhou, F., Wang, X., Jan, P., Dumas, P., Peng, S., Li, L., Zhou, X., & others. (2021). Irrigation, damming, and streamflow fluctuations of the Yellow River. *Hydrology and Earth System Sciences*, *25*(3), 1133–1150.
Yu, Z., Pollard, D., & Cheng, L. (2006). On continental-scale hydrologic simulations with a coupled hydrologic model. *Journal of Hydrology*, *331*(1–2), 110–124.
Yuan, X., Ma, F., Wang, L., Zheng, Z., Ma, Z., Ye, A., & Peng, S. (2016). An experimental seasonal hydrological forecasting system over the Yellow River basin – Part 1: Understanding the role of initial hydrological conditions. *Hydrology and Earth System Sciences*, *20*(6), 2437–2451. https://doi.org/10.5194/hess-20-2437-2016